Materials Science-Poland, Vol. 23, No. 3, 2005

Electrical and optical properties of sol-gel derived ZnO:Al thin films

P. SAGAR, M. KUMAR, R.M. MEHRA*

Department of Electronic Science, University of Delhi, South Campus New Delhi, 110021, India

High quality sol-gel derived ZnO and ZnO:Al thin films were deposited on corning (7059) glass substrates by spin coating. The annealed films showed the *c*-axis-preferred orientation. The structural, electrical, and optical properties of the films were investigated as a function of Al concentration from 0 to 3.0 at. %. The maximum conductivity of 18.86 $\Omega^{-1}\cdot cm^{-1}$ with the carrier concentration of 2.2×10^{24} m^{-3} was found for the Al concentration of 0.8 at. %. The conductivity is found to be of the activated type above 375 K, and variable range hopping conduction is observed below room temperature. Various transport parameters, such as the average spacing between donors, effective Bohr radius, donor levels, Debye screening length, and average grain size, have been estimated. The increase in band gap with Al doping is explained in terms of a Burstein Moss shift.

Key words: *sol-gel; ZnO: Al, spin coating; transport parameters*

1. Introduction

Zinc oxide (ZnO) is an interesting wide-band-gap semiconductor material with a direct band gap of 3.36 eV [1] at room temperature and exciton binding energy of 60 meV. It has crystalline structure of the wurtzite type and the unit cell with the constants a = 3.24 Å and c = 5.19 Å. Thin films of undoped and doped ZnO are utilized for a wide variety of electronic and opto-electronic applications, such as surface acoustic wave devices [4], transparent conducting electrodes [2], heat mirrors [3]. Nanoscale porous structures of ZnO with a high surface area find their application in chemical sensors [5] and dye-sensitised solar cells [6]. Various techniques have been used to deposit undoped and doped ZnO films on different substrates, including spray pyrolysis [7], organometallic chemical vapour deposition [8], pulsed laser deposition

*Corresponding author, e-mail: rammehra@netscape.net

[9], sputtering [10], and sol-gel process [11]. Among these, the sol-gel technique is credited with several advantages, such as deposition of high purity, homogeneous, cheaper, large-area films at relatively low temperatures. There are scarcely any reports on the transport parameters of ZnO:Al films prepared by the sol-gel technique.

In this paper, we concentrate on the structural, electrical conductivity and optical properties of sol-gel derived ZnO and ZnO:Al films deposited by spin coating. Estimates of various transport parameters, such as the average spacing between donors (r), effective Bohr radius (a^*), donor levels (E_d), Debye screening length (L_D), and average grain size (l), have been made.

2. Experimental details

The solutions were prepared by dissolving zinc acetate, $Zn(CH_3COO)_2 \cdot 2H_2O$ (purity 99.95%), in anhydrous methanol in increasing Al doping concentrations (98.5% purity $AlCl_3$) ranging from 0 to 3 at. %. The obtained mixture was mixed ultrasonically for about two hours. The solutions became turbid within twenty four hours after preparation. The turbidity was removed using 0.2 micron filters. The substrates were cleaned ultrasonically, first in acetone, and subsequently in methanol for 10 minutes each. They were further cleaned with ion exchanged distilled water for 20 minutes and kept in an oven at 80 °C for 30 minutes. The clear solutions were used for spin coating after 24 hours on corning glass (7059) substrates. The films were first dried at 80 °C and then at 300 °C for 20 minutes each. This process was repeated several times to deposit films of the desired thickness. The films were annealed for half an hour at temperatures from 500 to 600 °C for decomposition and oxidation of the precursors. Diffraction patterns of intensity versus 2θ were recorded with a Philips PW 1830 diffractometer, using a monochromatized X-ray beam with nickel-filtered Cu_kR radiation (λ = 1.5418 Å). A continuous scan mode was used to collect 2θ data from 20 to 60°, with a 0.02 sample pitch and 4 deg·min^{-1} scan rate. The thickness of the films was found to be ≅ 0.14–0.2 μm, as determined by a DEKTECK^{3-ST} surface profilometer. The surface morphology of the films was analysed by Scanning Electron Microscopy (SEM) with a JEOL JSM-6300, and atomic force microscopy (AFM) using an SPI 3700. Optical transmittance measurements were carried out using a Shimatzu UV-260 spectrophotometer. The electrical conductivity (σ) and the Hall coefficient (R_H) were measured by the van der Pauw [12] technique. The sign of the Hall coefficient confirmed the n-type conduction of the films. The carrier concentration (n) and the Hall mobility (μ_H) were determined using the expression $R_H = 1/ne$ and $\mu_H = R_H \times \sigma$, respectively. It should be mentioned that experimental data were reproducible with the accuracy of nearly 1.0%.

3. Results and discussion

3.1. Structural properties

ZnO:Al films were fabricated by the sol-gel technique on Corning glass substrates, and the XRD spectra of the ZnO and ZnO:Al films annealed in the temperature range 525–600 °C were gathered. Figure 1 shows the XRD patterns of ZnO and ZnO:Al films deposited at different Al dopant concentrations and annealed at 575 °C. The films exhibit a dominant peak at $2\theta = 34.34°$ corresponding to the (002) plane of ZnO, and other peaks corresponding to (100) and (101) and indicating the polycrystalline nature of the films. It is seen from the figure that the relative intensity of the (002) peak increases with increasing Al dopant concentration up to a concentration of Al equal to 0.8 at. %, and thereafter it starts to decrease. The increase in peak intensity indicates an improvement in the crystallinity of the films.

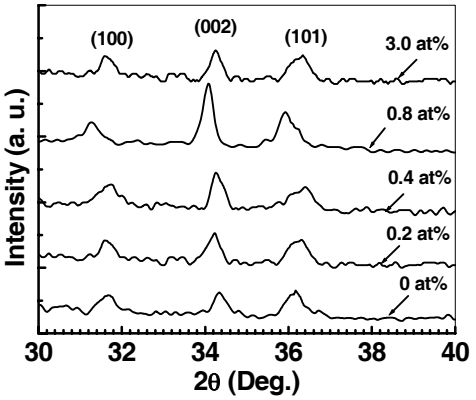

Fig. 1. X-ray diffraction patterns of ZnO and ZnO:Al films with various Al concentrations and annealed at 575 °C in air

Figure 2 shows the variation of the grain size l and texture coefficient TC with Al concentration. The extent of the preferred orientation as compared to other observed orientations is defined by the TC as [13]

$$TC(hkl) = \frac{\dfrac{I(hkl)}{I_0(hkl)}}{\dfrac{1}{N}\sum_N \dfrac{I(hkl)}{I_0(hkl)}} \tag{1}$$

where $I(hkl)$ is the measured relative intensity of the diffraction peak corresponding to hkl and $I_0(hkl)$ is the relative intensity peak corresponding to plane of ZnO powder. The increase in the texture coefficient of the film with an Al concentration of 0.8 at. % indi-

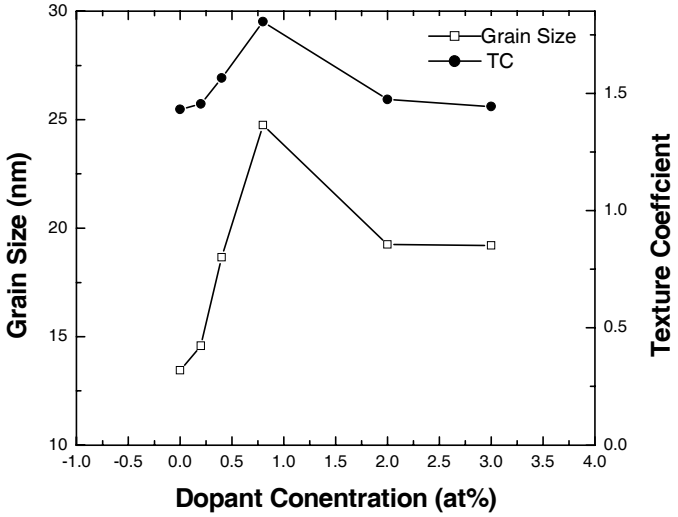

Fig. 2. Variation of the grain size *l* and texture coefficient *TC* with Al dopant concentration

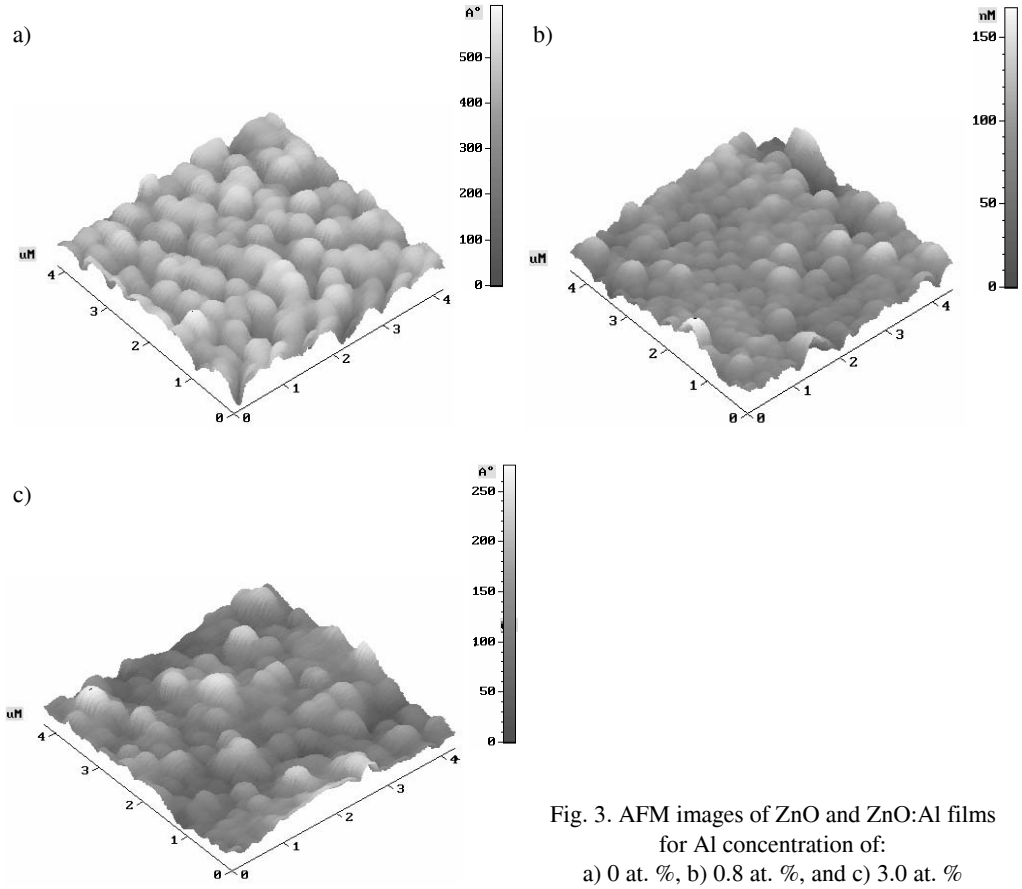

Fig. 3. AFM images of ZnO and ZnO:Al films for Al concentration of: a) 0 at. %, b) 0.8 at. %, and c) 3.0 at. %

cates that a large number of crystallites are oriented along the *c*-axis. The grain size of the films was estimated from the Scherrer formula [14] using the FWHM of the peak corresponding to (002) plane. The grain size was found to increase from 13 nm (undoped) to a maximum of ~25 nm for an Al concentration of 0.8 at. %. At 3.0 at. % of Al, the grain size was reduced to 19 nm. The scanning electron microphotograph of the film with an Al concentration of 0.8 at. % shows uniformly distributed grains with a smaller number of voids.

Figure 3a–c shows AFM images of ZnO:Al films with an Al dopant concentration of 0.0, 0.8, and 3.0 at. %, respectively. The RMS value of the surface of the undoped ZnO film is 22 nm whereas for the film having 0.8 at. % of Al it is 4.3 nm. At a higher Al dopant concentration (3.0 at. %), the surface was found to be rough (RMS = 86 nm). Thus, this study of structural properties reveals that the film doped with 0.8 at. % of Al is smooth and highly oriented along the *c*-axis oriented with densely packed grains.

3.2. Electrical properties

The values of R_H at different concentrations of Al are given in Table 1. The variations of σ_{RT}, n, and μ_H with Al concentration in ZnO:Al films are shown in Fig. 4. It is seen from this figure that σ_{RT} and μ_H increase with increasing Al concentration. Maximum values of σ_{RT} (18.86 $\Omega^{-1}\cdot cm^{-1}$) and μ_H (52.8 cm^2/Vs) are obtained for 0.8 at. % of Al. With further increase in Al concentration (> 0.8%), σ_{RT} and μ_H are found to decrease. Minami et al. [15] have also reported the value of $\mu_H \cong 45$ cm^2/Vs in Al doped ZnO films.

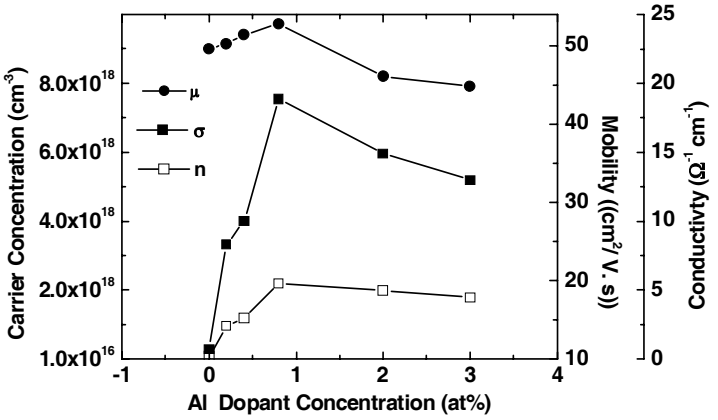

Fig. 4. Carrier concentration n, Hall mobility μ, and resistivity ρ of ZnO:Al films annealed at 575 °C in air as a function of Al concentration

The carrier concentration in the doped ZnO film increases linearly with increasing dopant concentration up to 0.8 at. %. The observed increase in n and μ_H with dopant

concentration up to 0.8 at. % accounts for the increase in conductivity in accordance with the relation $\sigma = ne\mu_H$. The overall variation in n and μ_H can be understood in terms of the position of Al in the ZnO lattice. The ZnO film generally grows as an n-type semiconductor, due to the presence of native defects in the form of zinc interstitials, oxygen vacancies, or both. The observed behaviour at low doping levels (up to 0.8 at. % of Al) is expected to be the result of substitutional doping of Al^{3+} at Zn^{2+} sites, which creates one extra free electron in the conduction band. A decrease in n and μ_H at higher dopant concentrations (> 0.8 at. %) may be due to the interstitial occupancy of Al in the ZnO lattice, which may lead to a distortion of the crystal structure. The presence of Al at interstitial sites and grain boundaries in the form of oxide, besides decreasing grain size, may act as scattering centres and result in a decrease in the observed mobility at dopant concentration > 0.8 at. %. XRD results also suggest the degradation of film structure at higher dopant concentrations.

Table 1. Activation energy at high temperatures E_a, average spacing between donors r, r/a^*, Debye screening length L_D, activation energy of grain boundary limited conductivity E_σ, the change ΔE_g in E_g, and absorption edge shift ΔE^{BM} at different Al dopant concentrations

Dopant conc. (at. %)	E_a (eV)	r (nm)	r/a^* (nm)	L_D (nm)	E_σ (eV)	ΔE_g (eV)	ΔE^{BM} (eV)	R_H (cm^3/C)
0.0	0.94	12	8.3	13.5	0.96	–	–	70.4
0.2	0.82	6.2	4.3	4.0	0.86	0.015	0.011	6.4
0.4	0.66	5.8	4.0	3.6	0.67	0.018	0.013	5.2
0.8	0.43	4.7	3.2	2.7	0.47	0.025	0.020	2.8

Structural surface morphology and electrical studies indicate that films with higher concentrations of Al (> 0.8 at %) are two-phase solids. These films may contain clusters of an Al-rich phase, but not Al^{3+} ions in the interstitials position. Therefore, studies of the temperature variation of electrical conductivity and optical properties are restricted to films containing Al up to 0.8 at %.

The dependence of conductivity ($\ln\sigma$ vs. $10^3/T$) for a ZnO:Al film at high temperatures (375–475 K) is shown in Fig. 5. It is observed that $\ln\sigma$ vs. $1/T$ curves are linear in this temperature range, indicating an activated conduction process following the expression

$$\sigma = \sigma_1 \exp\left(-\frac{E_a}{kT}\right)$$

The activation energies E_a listed in Table 1 are found to decrease with increasing dopant concentration up to 0.8 at. %.

In Figure 5, conductivity variation with temperature in the range of 153–600 K for an undoped ZnO film is also shown as an insert. The data below room temperature

were analysed assuming Mott's variable range hopping conduction process [16]. As shown in Fig. 6, $\ln(\sigma T^{1/2})$ vs. $1/T^{-1/4}$ plots are linear, indicating variable range hopping (VRH) conduction.

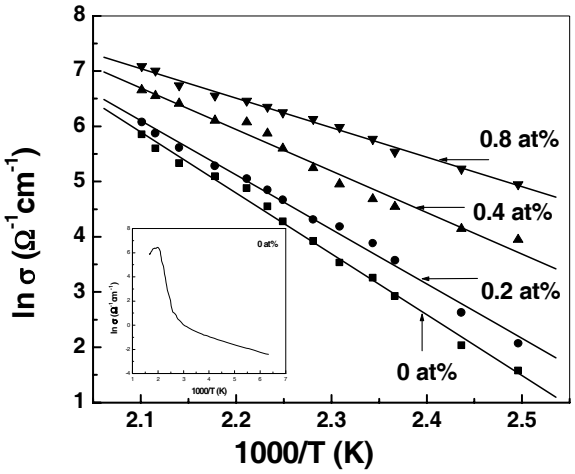

Fig. 5. Arrhenius plot of the DC conductivities σ of ZnO and ZnO:Al films with different Al concentrations

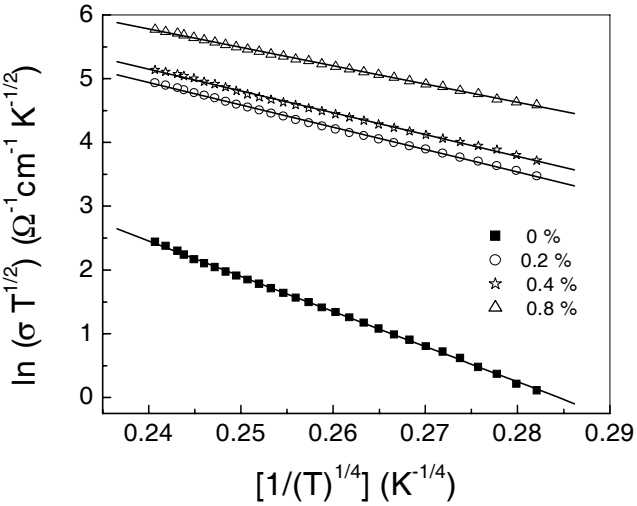

Fig. 6. Plot of $\ln(\sigma T^{1/2})$ versus $T^{-1/4}$ for ZnO and ZnO:Al films with different Al concentrations

Hausmann and Teuerle [17] have classified three types of conduction process in indium-doped single crystals at low temperatures (below 300 K), depending on the ratio of the average spacing between donors r to the effective Bohr radius a^*. The values of r and a^* are given as

$$r = \left(\frac{4\pi N_d}{3} \right)^{-1/3} \tag{2}$$

$$a^* = \frac{a_0 \varepsilon_s m}{m^*} \tag{3}$$

where N_d is the impurity concentration, m is the mass of a free electron, m^* is the effective mass of the electron, ε_s is the relative electric permittivity, and a_0 is the Bohr radius:

$$a_0 = \frac{4\pi\varepsilon_0 \hbar^2}{me^2} = 0.53 \text{ Å}$$

• For $r/a^* > 5$, impurity concentration is low and impurity levels are isolated, while the conduction is explained by charge transport in the conduction band and nearest neighbour hopping between isolated donor levels.

• For $2 < r/a^* < 5$, called the intermediate concentration region, an impurity band is formed by the overlapping wave functions of donors. Therefore, a variable hopping conduction [18] appears between localized states in the impurity band.

• For $r/a^* < 2$, which is the high impurity concentration regime, metallic conduction takes place due to the overlapping of impurity and conduction bands.

The value of r in a doped ZnO film were estimated from Eq. (2), assuming that all donor atoms are ionised and completely contributing their charge carriers to the conduction band at least up to a dopant concentration of 0.8 at. %. The estimated values of r are given in Table 1 and found to decrease from 12.0 nm to 4.7 nm for dopant concentration of 0 and 0.8 at. %, respectively. This decrease in r is attributed to the enhanced substitution of Zn^{2+} by Al^{3+} and increasing concentration of charge carriers in the conduction band. The energy of the donor level of Al in the ZnO lattice E_d can be estimated using the expression

$$E_d = \frac{E_i m^*}{\varepsilon_s{}^2 m} \tag{4}$$

where E_i is the ionisation potential for Al (the energy required to completely remove an electron from the atom). Taking $E_i = 5.984$ eV [19], $m^* = 0.31$ m, and $\varepsilon_s = 8.5$ [19] for ZnO, we obtain the value of $E_d = 25.67$ meV. The values of r, a^* (Eqs. (2) and (3)), and r/a^* are also included in Table 1. It is seen from this table that the ratio r/a^* lies between 2 and 5, which suggests VRH conduction between localized states in the impurity band. The observed value of $E_d = 25.67$ meV for Al in a ZnO lattice also suggests that all impurities will be ionised above RT, and therefore VRH conduction is possible below RT only to the extent observed in the present case.

The effect of grain boundaries on electron transport in the conduction band can be examined by comparing the Debye screening length L_D with the average grain size l. L_D can be expressed as [20]

$$L_D = \left(\frac{\varepsilon_s \varepsilon_0 kT}{e^2 N_d} \right)^{1/2} \tag{5}$$

where ε_s is the relative electric permittivity, ε_0 is the electric permittivity of free space and N_d is the donor concentration. Providing L_D is smaller than $l/2$, a potential barrier around each grain boundary is formed due to band bending. If, however, L_D is larger than $l/2$, the conduction band becomes flat and loses the potential barrier. Electrons are then transported without grain boundary scattering.

L_D for the doped films at 400 K is determined to be in the range 4.0–3.0 nm, while l, as estimated from the FWHM of the XRD peak using the Scherrer formula, lies in the range 13–25 nm (Table 1). It is seen from Table 1 that $L_D < l/2$, which suggests that the effect of the grain-boundary potential barrier on conduction at high temperatures may also be taken into account. The conductivity in this case can be represented as [21]

$$\sigma = \left(\frac{e^2 l N_d}{2\pi m^* kT} \right)^{1/2} \exp\left(-\left(\left(E_C - E_F \right) + e\phi \right) / kT \right) \tag{6}$$

where E_C is the energy of the conduction band minimum, E_F the Fermi level, ϕ the grain boundary potential barrier, and N_d the donor concentration. Assuming

$$E_\sigma = E_C - E_F + e\phi$$

as the activation energy for the grain boundary limited conductivity, the above equation can be written as

$$\sigma T^{1/2} \propto \exp\left(-\frac{E_\sigma}{kT} \right) \tag{7}$$

From the linear plot of ln ($\sigma T^{1/2}$) and T^{-1}, values of E_σ were obtained, and are listed in Table 1. The value of $E_\sigma / E_a \sim 1$ suggests thermionic emission over the grain boundaries at high temperatures in doped ZnO films. Thus, conductivity at higher temperatures depends on the morphology, i.e. the polycrystallinity of films.

3.3. Optical properties

Typical UV transmittances for 0 and 0.8 at % of Al are shown in Fig. 7. It is seen from this figure that the average transmittance T in the visible region is higher than 85% for films having 0.8 at. % of Al.

The optical band gap E_g was calculated using Tauc's plot (($\alpha h\nu$)^2 vs. $h\nu$), as shown in Fig. 8. The value of α is determined from transmittance spectra. The photon energy at the point where ($\alpha h\nu$)^2 is zero represents E_g, which is determined by extrapolation. An increase in E_g with Al doping up to 0.8 wt% is observed. It should be mentioned

that both the average transmittance and band gap are found to decrease at higher Al doping concentrations. The change ΔE_g in E_g with dopant concentration is also listed in Table 1.

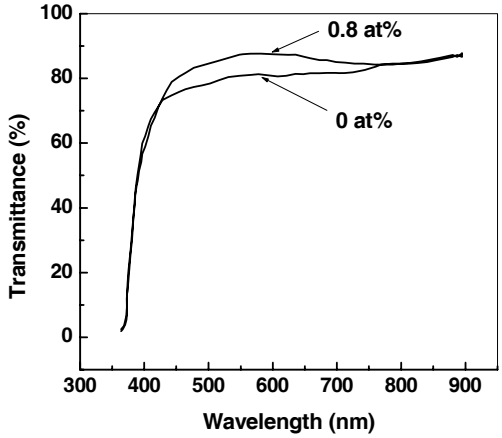

Fig. 7. Variation of transmittance T as a function of Al concentration in the wavelength range of 200–800 nm for ZnO and ZnO:Al films annealed at 575 °C

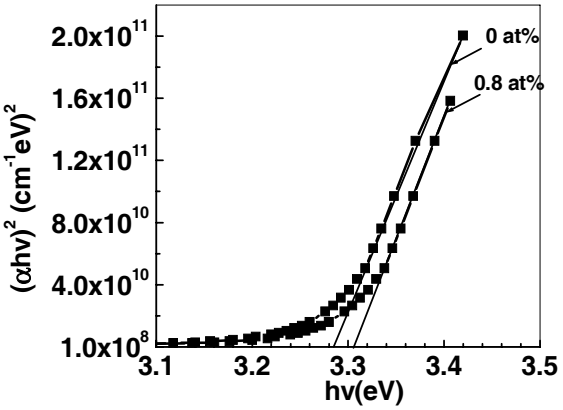

Fig. 8. Band gap E_g estimation for ZnO and ZnO:Al films using Tauc's plot

The dependence of E_g on carrier concentration is analysed considering the Burstein Moss (BM) model [22] for the absorption edge shift ΔE^{BM} in an n-type semiconductor, which is given by

$$\Delta E^{\mathrm{BM}} = \left(3\pi^2 N\right)^{2/3} \frac{\hbar^2}{2m_{vc}^*} \tag{8}$$

where m_{vc}^* is the reduced effective mass [23] given by

$$\frac{1}{m_{vc}^*} = \frac{1}{m_c^*} + \frac{1}{m_v^*} \tag{9}$$

where m_c^* is the effective mass in the conduction band and m_v^* is the effective mass in the valence band. The variation of ΔE_g and ΔE^{BM} with n is shown in Fig. 9, from which it is seen that the BM shift accounts fairly well for the observed change in the band gap.

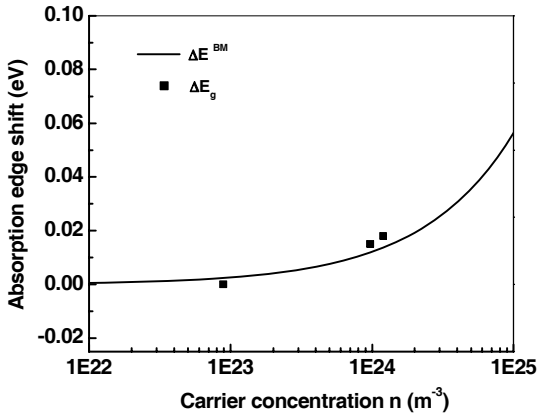

Fig. 9. Absoption edge shift as a function of carrier concentration. The solid line shows the calculated ΔE^{BM}, ■ shows the experimental ΔE_g due to the variation in Al concentration

4. Conclusions

Highly conducting and transparent sol-gel derived ZnO:Al films have been deposited by spin coating. It has been found that the *c*-axis orientation and grain size of the films significantly depend on Al concentration. The analysis of the peak intensity (texture coefficient) and FWHM of the XRD spectra clearly indicate that at the critical dopant concentration (0.8 at. % of Al) the film contains a maximum number of crystallites oriented along the *c*-axis and exhibiting a large grain size. Conductivity data suggest different conduction mechanisms at high and low temperatures. At high temperatures, electrical transport in ZnO:Al films is attributed to the grain boundary potential barrier, which is also confirmed from the estimated Debye screening length and average grain size ($L_D < l/2$). The observed VRH conduction at low temperatures is ascertained from the calculated ratio of the average spacing between donors to the effective Bohr radius ($2 < r/a^* < 5$). The change in band gap due to Al doping is ascertained due to BM shift.

Acknowledgements

The authors wish to acknowledge the financial support of DRDO, Govt. of India, India.

References

[1] BIXIA LIN, ZHUXI FU, YUNBO JIA, Appl. Phys. Lett., 79 (2001), 943.
[2] SRIKANT V., CLARKE D.R., J. Appl. Phys., 81 (1997), 6357.
[3] MINAMI T., NATO H., TAKATA S., Thin Solid Films, 124 (1985), 43.
[4] CHOPRA K.L., MAJOR S., PANDAY D.K., Thin Solid Films, 102 (1983), 1.
[5] WEIBENRIEDER K.S., MULLER J., Thin Solid Films, 300 (1997), 30.
[6] SEOK-SOON KIM, JUN-HO YUM, YUNG-EUN SUNG, Solar Energy Mat. Solar Cells, 79 (2003), 495.
[7] NUNES P., FORTUNADEO E., MARTINS R., Thin Solid Films, 383 (2001), 277.
[8] ROTH A.P., WILLIAMS D.F., J. Appl. Phys., 52 (1981), 6685.
[9] LU Y.F., NI H.Q., MAI Z.H., REN Z.M., J. Appl. Phys., 88 (2000), 498.
[10] JIANG X., WONG F.L., FUNG M.K., LEE S.T., Appl. Phys. Lett., 83 (2003), 1875.
[11] JIMENEZ-GONZALEZ A.E., URUETA J.A.S., SUAREZ-PARRA R., J. Crystal Growth, 192 (1998), 430.
[12] VAN DER PAUW L.J., Philips Res. Repts., 13 (1958), 1.
[13] BARRED C., MASSALSKI T.B., *Structure of Metals*, Pergamon Press, Oxford, 1980, p. 204.
[14] LI B.S., CHU Y.S., SHEN D.Z., LU Y.M., ZHANG J.Y., FAN X.W., J. Appl. Phys., 91 (2002), 501.
[15] MINAMI T., NANTO H., TAKATA S., Thin Solid Films, 124 (1985), 43.
[16] LEE M.J.G., Phys. Rev., 187 (1969), 901.
[17] HAUSMANN A., TEUERLE W., Z. Phys., 257 (1972), 299.
[18] MOTT N.F., J. Non-cryst. Solids, 1 (1968), 1.
[19] KIREEV P.S., *Semiconductor Physics*, Chap. 2, 2nd Ed., Mir Publication, 1975, p. 150.
[20] ORTON J.W., POWELL M.J., Rep. Prog. Phys., 43 (1980), 1263.
[21] SETO J.Y.W., J. Appl Phys. 46 (1975), 5247.
[22] BURSTEIN E., Phys. Rev., 93 (1954), 632.
[23] SINGH A.V., MEHRA R.M., YOSHIDA A., WAKAHARA A., J. Appl. Phys., 95 (2004), 3640.

Received 21 May 2004
Revised 29 June 2005